CLM-P779

CLM-P779

UKAEA

Preprint

REDUCED MHD MODELLING OF TEARING MODE INTERACTIONS IN TOKAMAKS

J. W. Eastwood
W. Arter

CULHAM LABORATORY
Abingdon, Oxfordshire
1986

CLM-P 779

REDUCED MHD MODELLING OF TEARING MODE INTERACTIONS IN TOKAMAKS

James W.Eastwood and Wayne Arter

Culham Laboratory, Abingdon, Oxfordshire, OX14 3DB, UK

(EURATOM/UKAEA Fusion Association)

Abstract

A series of three dimensional reduced MHD simulations has been undertaken to investigate the nonlinear tearing mode interaction mechanism widely believed to explain hard disruptions in tokamaks. Validation of the computations has taken into account both linear and nonlinear numerical stability. Linear stability and energy conservation are shown to be necessary for convergence. Many features of simulations of 'hard disruptions' bear out our theory of a spurious finite time singularity. Adjusting numerical and/or physical parameters suppresses the nonlinear instability as predicted, thus allowing calculations to be pursued indefinitely. The sensitivity of converged calculations to variations of number of modes, initial and boundary conditions has been studied. Mode interactions are insensitive to parameter variations; large amplitude tearing modes lead to transient Alfvén wave bursts, with the persistence of the bursts being greater for fixed boundary voltage calculations.

(Submitted for publication in Physics of Fluids)

May 1986

I. INTRODUCTION

It is widely believed that resistive magnetohydrodynamic (MHD) effects, in the form of tearing modes, play a major role in the disruptive termination of tokamak discharges. This continues to be an active area of research.[1,2] A tearing mode involves a change in the topology of magnetic field lines which converts parts of the field energy into kinetic and thermal energy. Typically, the magnetic field is little changed outside a narrow "island region", where the driven fluid motion also tends to be concentrated. MHD theories of disruptions are of two basic kinds: one sort relies on the interaction of transport effects with tearing modes[3,4] and the other invokes the interaction of tearing modes of different helicities[5,6,7].

The first assumes the current density at the centre of the tokamak plasma to be limited by sawtooth activity or the accumulation of impurities. In these circumstances, a small increase in total current or change in the spatial variation of the resistivity may lead to a situation where the magnetic islands just keep on growing, provided the associated transport effects are allowed to feed back into the resistivity. Ultimately the islands become so large that collectively they cover the effective plasma minor radius, and the associated thermal transport from the centre to the edge then rapidly cools the discharge.

The second argues that when modes with (poloidal wavenumber, toroidal wavenumber)= (m,n) = (2,1) and (3,2) grow to sufficiently large amplitudes that the islands overlap, there is a destabilisation of the (3,2) and other low (m,n) modes on a timescale of the same order as the (2,1) linear mode growth rate. Subsequently a large number of high m modes are destabilised, leading to explosive growth. The final phase of the

calculations show approximate energy equipartition amongst high m modes, rapid growth rates and the results becoming independent of resistivity.

In this paper we focus our attention on the nonlinear tearing mode interaction mechanism. In common with other authors, we assume initial profiles which are strongly unstable to tearing modes.[5,6,8] Although some workers think it plausible that such profiles could develop,[9] as far as we are aware, no numerical simulations have been undertaken which demonstrate the necessarily rapid profile modification to justify the very unstable initial conditions. Experimental data does not give conclusive evidence on this point. Our efforts to fit profiles to experiment showed both stable and unstable profiles to fit within experimental error bars. Consequently, we regard the question of how the initial state was arrived at as subject to further investigation.

The 'disruption' in the three-dimensional numerical simulations is loosely defined. Experimentally observed characteristics, the negative loop voltage spike, increased magnetic activity, temperature collapse and subsequent current loss are only partially reproduced. The majority of MHD simulations undertaken have used constant voltage boundary conditions, so any variations in loop voltage have to be inferred from changes in the self inductance. The concept of thermal shorting through ergodic fields has led to island overlap being used as prognostic of disruptions[7]. Calculations performed at the large values of Lundquist number, $S \simeq 10^6$-10^8, characteristic of present day tokamaks have not continued long enough to demonstrate temperature collapse and current loss phases[6], so they do not justify the use of the prognostic.

The most notable feature of the simulations is that at sufficiently high S ($\sim 10^6$), explosive mode growth and approximate equipartition of energy amongst the high m modes follows the nonlinear interaction of

overlapping (m,n) = (2,1) and (3,2) helicity islands. In the 'hard' disruption cases, the cascade to short wavelengths is such that the calculations are unable to continue beyond the explosive phase. Several papers have used the inability to compute further as an indicator of disruption[6,7,10]. This we also regard as a possibly misleading prognostic, and indeed it will be shown that a completely different interpretation is consistent with the results.

The principal issue tackled in this paper is what happens to the reduced MHD model beyond the explosive growth phase. Is the further development consistent with experimental observation? Section II contains a description of the model equations and their discretisation. Sec.III gives results for the 'hard disruption' case, followed in Sec.IV by theoretical interpretation and predictions. Sec.V presents (computer) experimental tests of the predictions. Sec.VI gives results for stabilised 'disruptions', outlining sensitivity to dissipation, mode truncation and boundary conditions.

II. THE MODEL

A. Differential Equations.

The solely MHD mechanism is studied using the low beta reduced equations of Strauss[11], to which we add a plasma resistivity and viscosity, so that they become

$$\left(\frac{\partial}{\partial t} + \underset{\sim}{v}.\underset{\sim}{\nabla}\right)\psi = \eta j - \frac{\partial \phi}{\partial \zeta} - E^{w} , \qquad (1)$$

$$\left(\frac{\partial}{\partial t} + \underset{\sim}{v}.\underset{\sim}{\nabla}\right)U = - S^{2} \left(\underset{\sim}{e}_{\zeta}.\underset{\sim}{\nabla}\psi \times \underset{\sim}{\nabla} j + \frac{\partial j}{\partial \zeta}\right) + p_{m} \nabla_{\perp}^{2} U . \qquad (2)$$

ψ is the dimensionless poloidal magnetic flux function, U is the negative of toroidal vorticity and the other quantities are as defined by Hicks et al[12] except for the magnetic Prandtl number $p_m = \nu/\eta_o$ where ν is the plasma viscosity (assumed uniform) and η_o is a typical (dimensional) value of resistivity.

Viscosity is included for numerical reasons, although $p_m = 0(1)$ can be justified on physical grounds. p_m is equal to the ratio of the viscous to resistive decay times. Using Braginskii coefficients,[13] we may estimate p_m to be

$$p_m = \frac{4\pi\sigma_{\parallel}\,\eta_1}{n m_i c^2} \simeq \beta\sqrt{(m_i/m_e)} = 0(1)\ , \qquad (3)$$

where n, $m_i c^2$, $\sigma_{\parallel}$ and η_1 are as defined in ref.13 and β is the usual plasma β.

Eqns (1) and (2) have the energy conservation law

$$\frac{d}{dt}\int_V \frac{1}{2}\left\{\left|\underset{\sim}{\nabla}_\perp\psi\right|^2 + \rho\frac{\left|\underset{\sim}{\nabla}_\perp\phi\right|^2}{S^2}\right\} d\tau =$$

$$\int_{\partial V}(E_w+\dot{\psi})\underset{\sim}{\nabla}_\perp\psi\cdot d\underset{\sim}{\sigma} - \int \eta j^2 d\tau - \int\frac{p_m}{S^2} U^2\, d\tau\ . \qquad (4)$$

This is a statement that the rate of change of total magnetic and kinetic energy in volume V is given by the Poynting flux of magnetic energy through the surface ∂V of V less the joule and viscous dissipation. In Eq.(4), it is assumed that boundary conditions are such that there are no kinetic energy sources or sinks on ∂V. The $\nabla_\perp$ symbol indicates gradient operators with the toroidal (ζ) component absent.

B. Discrete Equations.

The large aspect ratio ordering leading to Eqs.(1) and (2) has reduced the description of the tokamak to a long thin cylinder with axis parallel to ζ. If the cylindrical polar coordinate system (r,θ,ζ) is employed, then a natural representation of Eqs.(1) and (2), and the associated constitutive (Poisson's) equations relating j to ψ and ϕ to U is in terms of the fourier series expansions of the periodic coordinates θ and ζ. i.e. $f(r,\theta,\zeta)$ is written as:-

$$f(r,\theta,\zeta) = \sum_{m,n} \tilde{f}_{m,n}(r)\exp\left[i\left(m\theta + \frac{n\zeta}{R_o}\right)\right] . \qquad (5)$$

Using the expansion, Eq.(5), for variables appearing in Eqs.(1) and (2), and projecting the resulting equation onto the space spanned by a finite set of modes $\{(m_i,n_i);\ i\ \varepsilon[1,N_m]\}$ leads to a set of N_m coupled equations for the harmonic amplitudes. These differential equations (in r and t) are a spectral approximation to Eqs.(1) and (2), and they retain exactly the conservation law, Eq.(4), provided functions appearing in Eq.(4) are interpreted as their truncated fourier series approximations.

The spectral equations, which are differential in r and t, are converted into discrete equations by finite differencing in r and t. Second order accurate space centred difference approximations to radial derivatives and two-step time derivative approximations (forward followed by backward Euler differencing) are used[14]. These equations are implemented in the code FORBAK, which was developed from the RSF code[12]. FORBAK uses the same methods for evaluating convolutions and solving Poisson's equation as RSF.

C. Stability and Convergence.

To resolve the possible spectrum of Alfvén modes completely, it may be argued that ~ S mesh points (or modes) are required for each dimension, and calculations need to be pursued for a time which scales as some fractional power of S. If this pessimistic view held, then computer time required to undertake tokamak simulations would scale as S^{γ}, where $\gamma \simeq 6$, and any predictive computations would be impractical. Fortunately, the scaling with S does not appear in reality to be so severe, although computer resources still constrain the accessible range of parameters (S, p_m).

The question of stability and convergence of the simulation results can be tackled in three stages; linear stability, convergence to the spectral approximation and structural stability of the solution of the spectral equations. These stages respectively determine the appropriate timestep Δt, radial mesh spacing Δr and number of helical modes N_m.

A local stability analysis following the procedure used in ref.15 gives for the equations used in FORBAK the following timestep criterion

$$\max\left\{\sqrt{3}S\left|\underset{\sim}{k}\cdot\underset{\sim}{B}\right| + \left|\underset{\sim}{k}\cdot\underset{\sim}{v}\right|\right\} \Delta t \leq 2 \qquad (6)$$

(c.f. RSF[12,14,15] where a nonzero viscosity is required for a bound with $\Delta t \neq 0$ to exist). A practical implementation of inequality (6), choosing Δt to satisfy at each timelevel

$$\max_j \{\sqrt{3}\, S\Big[\sum_{mn} \Big(\frac{\pi\left|m\tilde{\phi}_{m,n}\right|_j}{r_j \Delta r_j} + M^* \left|\frac{\partial \tilde{\psi}_{m,n}}{\partial r}\right|_j\Big) + N^*\Big]$$

$$+ \sum_{mn} \Big(\pi \frac{\left|m\tilde{\phi}_{m,n}\right|_j}{r_j \Delta r_j} + M^* \left|\frac{\partial \tilde{\phi}_{mn}}{\partial r}\right|_j\Big)\} \Delta t = \alpha \qquad (7)$$

has been found to maintain linear stability with $\alpha = 1$. (M^*, N^*) are the maxima of mode numbers (m,n), and j is the index labelling radial mesh points.

The nonlinear instabilities[16,17] (finite time singularity), arise because of insufficient spatial resolution in the radial coordinate. It follows from the Ritz-Galerkin (spectral) approximation used to discretise and θ and z coordinates that

In the limit $\Delta r \to 0$, $\Delta t \to 0$, where Δr and Δt are such that inequality (6) is satisfied, energy, as defined by Eq.(4) with functions approximated by truncated fourier series (Eq.(5)), is conserved.

This theorem holds for any number of helical modes. It is of great practical importance in that it allows us to separate convergence of the difference equations to the mode truncated reduced MHD equations from considerations of structural stability; conservation of total energy as $\Delta r, \Delta t \to 0$ provides a simple scalar measure of convergence for a given number of modes. The structural stability of the converged mode truncated solutions can then be investigated by varying the number of modes.

III. THE 'HARD' DISRUPTION

For single helicity calculations, the initial phase of exponential

growth is followed by the nonlinear Rutherford[18] regime, where islands grow linearly in time whilst maintaining approximate force balance. Saturation is reached[9,19] when the poynting flux of energy into the island is balanced by the joule (and if present viscous) dissipation. The same pattern is followed by islands which saturate with small widths in multihelicity calculations.

Multihelicity calculations starting from an equilibrium that is linearly highly unstable to the (m,n) = (2,1) and (3,2) tearing modes are significantly different. These modes interact in the Rutherford regime, to increase the growth rate of the (3,2) mode, by profile modification[3,20] or by nonlinear interactions through the (5,3) mode[21]. Subsequently, a large number of high m modes are destabilised, leading to a phase of explosive growth.[7]

Following the excitation of the large number of modes:[7,22]

i) there is approximate equipartition of energy among high m modes,

ii) most of the modes grow with similar growth rate and,

iii) results become independent of resistivity.

Computations which exhibit this explosive growth are commonly described as 'hard disruption' cases. Features i) - iii) appear in the last phase of the calculation[7]; Computations are unable to proceed either because overflow is encountered, or as is the case with FORBAK, the timestep becomes vanishingly small.

An example of a 'hard disruption' case is shown in Fig.1. The physical parameters chosen for this case follow those of Ref.6 apart from the choice of boundary condition. $S = 10^6$, $p_m = 0$, uniform density profile, $\rho(r) = 1$, constant current boundary conditions and an initial q profile given by

$$q(r) = q_o \left(1 + \left(\frac{r}{r_o}\right)^{2\lambda}\right)^{1/\lambda} , \qquad (8)$$

where $q_o = 1.34$, $r_o = 0.567$ and $\lambda = 3.24$. An initial static equilibrium was obtained by setting $\eta(r,t = 0) = E_w/j(r,t = 0)$. Numerical parameters used were $N_g = 100$ radial mesh points, 11 modes $(m,n) = \{(0,0),(1,0),(1,1),(2,1),(3,2),(5,3),(4,2),(6,3),(6,4),(7,4),(8,4)\}$. The axisymmetric initial equilibrium was perturbed by approximations to islands of widths $w_{m,n}$, where $w_{2,1} = w_{3,2} = 0.05$, $w_{5,3} = 0.01$ measured in units of the minor radius a, and $w_{m,n} = 0$ otherwise. Figure 1a shows the evolution of energies in the dominant (2,1) mode and the discrepancy, ΔE_T, in the total energy budget:

$$\Delta E_T = \int_o^t (\dot{M} + \dot{K} + P + J + W)\, dt' , \qquad (9)$$

where M and K are respectively total magnetic and kinetic energies, P,J, and W are total poynting, joule and viscous powers. In FORBAK, Eq.(9) is numerically evaluated for the finite difference/spectral equations used. It follows from Sec.II that for sufficiently small Δr and Δt, ΔE_T can be made arbitrarily small. In the latter stages of the calculation (after island overlap, cf.figure 1b), ΔE_T is not negligible. Eventually it becomes as large as the magnetic energy in the (2,1) mode. This remains true even if α (Eq.(7)) is reduced, indicating that insufficient spatial resolution is the limiting factor.

The breakdown of energy conservation is reflected in the plots of the loop voltage evolution. The curve labelled 'direct measure' in Fig.1c is the loop voltage measured at the boundary (r = a)

$$V = \frac{P}{2\pi I} \qquad (10)$$

whereas the 'indirect measure' curve uses the formula:

$$V = -\frac{1}{2\pi I}\left(\dot{M} + \dot{K} + J + W\right) . \qquad (11)$$

For converged calculations ($\Delta E_T \to 0$), these two measures become identical.

Figure 1d is a log-log plot of energies versus time. The time t_o is the time at which the timestep became zero (to roundoff). Superimposed on the plot is a line of slope 2; this shows that in the final stage of the calculation, energy growth closely fits the law $E \propto (t_o - t)^{-2}$.

Finite time singularities are observed over the range of parameters for which 'hard disruptions' are seen. Fig.2 shows results for less severe parameters than those of figure 1: $S = 10^5$, $p_m = 1$, constant voltage boundary conditions, initial profile parameters $q_o = 1.344$, $r_o = 0.56$, $\lambda = 3.24$. A time independent mass density profile, $\rho(1) = 1 - r^2 + r^4/2$ was assumed to provide direct comparison with more recent published results[22]. Initial perturbed island widths $w_{2,1} = 0.01$ and $w_{3,2} = w_{5,3} = 0.001$. The 57 modes used in the calculation are shown in Table I.

Figure 2a shows that the mode energies behave similarly to corresponding energies in figure 1a, but energy conservation is, as expected, considerably better. Even so, the computations are terminated by a finite time singularity. Fig.2b shows a selection of mode energies versus time, again exhibiting the $\propto (t_o - t)^{-2}$ asymptotic behaviour.

IV. NONLINEAR THEORY PREDICTIONS

A The Failure Mechanism

One interpretation of the hard disruption results is furnished by a theory we have developed[16]. In this theory, it is shown that there is a nonphysical feedback mechanism which feeds energy from short to long wavelengths through aliasing[23]. Aliasing through insufficient radial

resolution in finite difference/spectral reduced MHD equations has been shown to lead to finite time singularities of the form shown in Figs.1 and 2.

The essence of the theory for a closed system is as follows: Ignoring finite timestep effects, the finite difference/spectral equations, after suitable linear transformations, may be written symbolically as

$$\dot{x}_i = \alpha_{ijk} x_j x_k - \beta_{ij} x_j \quad , \tag{12}$$

where the set $\{x_i\}$ represents flux and vorticity function values and the summation convention is employed. The quadratic term in Eq.(12) corresponds to the nonlinear advection terms, and β_{ij} is a positive diagonal matrix describing the diffusion terms.

The energy conservation law becomes

$$\dot{E} = \frac{d}{dt}\left(\frac{x_i x_i}{2}\right) = \alpha_{ijk} x_i x_j x_k - \beta_{ij} x_i x_j \quad . \tag{13}$$

In the alias free limit, the symmetry of α_{ijk} is such that the cubic terms sum to zero, giving $\dot{E} \leq 0$. The same result holds (from Eq.(4)) for the differential system. This implies that in the alias-free limit, finite time singularities are impossible provided poynting fluxes remain bounded.

In the limit of small x_i, Eq.(12) yields solutions $x_i \sim \exp[-\beta_{ii} t]$ (no summation convention). For the large x_i asymptote, the linear term becomes negligible, and equations $\dot{x}_i = \alpha_{ijk} x_j x_k$ admit solutions of the form

$$x_i = X_i/(t_0-t) \tag{14}$$

where

$$X_i = \alpha_{ijk}X_jX_k \quad . \tag{15}$$

To prove that Eq.(14) gives singular solutions, we must demonstrate that there are real values $\{X_i\}$ satisfying Eq.(15). Accessibility of the singular solutions follows by showing that trajectories described by $\{X_i\}$ are attracting for $t_0 > 0$. We have proved both these points analytically (with the aid of the computer algebra program, MACSYMA[24]) for Alfvén wave solutions of particular spatial periodicity[16]. The analytic results have been verified and extended using standard ordinary differential equation solvers on solutions with particular spatial periodicities. Most significant features of the hard disruption results illustrated in Sec.III are as predicted by our theory:

i) from Eq.(14), amplitudes all grow as $(t_0-t)^{-1}$, giving the appearance of approximate equipartition of energy among the modes.

ii) Mode amplitudes grow with growth rate $\gamma \sim \dot{x}_i/x_i = 1/(t_0-t)$. i.e. modes have similar growth rates, and these rates become larger as t approaches t_0.

iii) Results become independent of resistivity. As $t \to t_0$, the ratio of advective to resistive terms tends to infinity: $\alpha_{ijk}x_jx_k/\beta_{ij}x_j \sim (t_0-t)^{-1}$.

iv) Energy conservation fails.

v) Asymptotically, energies grow as $(t_0-t)^{-2}$. The form of the quadratic terms in Eq.(1) is such that, more generally, one may expect magnetic energy $\propto (t_0-t)^{-2\delta}$; $0 \leq \delta \leq 1$ and kinetic energy $\propto (t_0-$

$t)^{-2}$, although only cases with $\delta=1$ have been observed using FORBAK.

B. Stability Boundaries

In addition to predicting the consequences of radial aliasing, our theory shows how to avoid them. For the simple particular periodicities and model problems that we were able to treat analytically, Lyapunov functions which give sharp estimates on the stable regions of parameter space can be constructed; These show that if we include sufficient dissipation, the unphysical singular behaviour is avoided. The amount of dissipation required is that which prevents energy cascade to subgrid scalelengths. Energy flows to shorter wavelengths through phase mixing and nonlinear coupling. The shortest scale lengths reached are determined by the balance between advective τ_a and diffusive τ_d timescales. To inhibit energy flow to length scales less that the grid spacing, Δr, we required $\tau_a/\tau_d < 0\ (1)$ at scale length Δr. For Alfvén wave processes, this implies a mesh Lundquist number

$$L_m = \frac{\tilde{V}_a \Delta r}{(\eta+\nu)} < 0(1) \quad , \tag{16}$$

and for flows, the mesh Reynolds number, R_e, and mesh magnetic Reynolds number, R_m, must also be small

$$R_e = \frac{\tilde{V}\Delta r}{\nu} < 0(1), \quad R_m = \frac{\tilde{V}\Delta r}{\eta} < 0(1) \quad . \tag{17}$$

$\tilde{V}_A$ and $\tilde{V}$ are measures of variations (e.g. peak-to-peak) of Alfvén and flow speeds.

Conditions (16) and (17) apply even in the limit $\Delta t \to 0$. They must be satisfied to guarantee avoiding the finite time singularities. If they are not avoided, then the $1/(t_0-t)$ growth of velocities will eventually lead to linear instability (cf.Eq.(7)) or cause $\Delta t \propto (t_0-t) \to 0$ as $t \to t_0$. The numerical values of the O(1) constants have not been found analytically, but can be estimated empirically. All we require here is to note that:

i) large transients and steep gradients make singular behaviour more likely,

ii) increasing η and/or ν stabilises and,

iii) decreasing Δr stabilises.

We verify ii) and iii) on the hard disruption cases below.

A second way to avoid these finite time singularities is to choose a numerical scheme which is free from them; one scheme of particular interest is EPIC[25].

V. NUMERICAL VERIFICATION

A. Increased Dissipation

Using the same initial conditions, radial mesh and number of modes as the case shown in Fig.1, we find that the singular behaviour disappears for p_m between 1 and 10. The physical effect of increasing viscosity is to reduce the growth rate of the large (m,n) islands and to make results generally smoother. However, apart from a renormalisation of timescales, evolution of the principal islands closely resembles the inviscid case up to the point where the inviscid case becomes singular.

Figure 3 shows island widths and loop voltages for a computation with mode selection and physical parameters identical to the case shown in Fig.1 apart from a changed magnetic Prandtl number. The direct and indirect voltage measures are almost indistinguishable for these cases, indicating improved energy conservation. The negative voltage spike, which reaches approximately the same magnitude as the equilibrium voltage, occurs as the island widths decay. Note that the peak negative voltage is larger for the case with larger viscosity.

B. Decreased Mesh-spacing

It may be argued that the cases of Figs.1 and 3 have too few modes. In addition p_m is too large in the example shown in Fig.3. Figure 4 shows results for 57 modes, $p_m = 1$, $S = 10^5$, where only the number of radial mesh points is changed. Plotted are energy errors versus time for the cases with 200 and 400 radial mesh-points. The 200 mesh-point case terminates at time $t_0 = .00704$ as the finite time singularity is approached. The converged results are discussed further below.

VI. THE STABILISED DISRUPTION

It follows from the results of Secs.IV and V that there exists a stable region of (S, p_m) parameter space which is free from unphysical singular behaviour, and that that region can be extended by employing finer radial meshes. Below, we describe what happens beyond the final phase of hard disruption cases when computations remain stable, and test the sensitivity of our results to parameter changes. For clarity, in this

section times are measured in Alfvén units, i.e. they are larger by a factor S than in the rest of the paper.

A. Structural Stability

For a given number of helical modes, our theory and computations suggest that once numerical instability is suppressed, the results become independent of radial mesh spacing. This section examines the structural stability of such solutions. By structural stability, we mean that a sufficiently large number of helical modes has been chosen so that the results of a converged computation do not change qualitatively with the addition of further modes.

To facilitate direct comparison, we focus our attention on the fixed voltage boundary condition, $S = 10^5$, $p_m = 1$, 57 mode case discussed in Secs. III and VB. Fig.5 shows the energy spectrum at four times during the simulation, and Fig.7a shows the corresponding inferred loop voltage V_I. The energy spectrum is dominated by modes with (2,1) helicity until time t = 630 (fig.5a). There is also a small amount of (3,2) energy which interacts with (2,1) to yield (1,1). Exponential growth of modes $(m,n) = k(2,1) \pm (3,2) = \ell(2,1) \pm 1/1$ then follows (those with the plus sign being favoured) and the spectrum rapidly broadens. After t = 630, all available modes contain significant energy and there is then a period when the spectrum advances towards equipartition. During this time, oscillations develop first in the energies of the highest (m,n) modes and then in lower (m,n) modes. Many of the modes contain almost equal magnetic and kinetic energy.

For times t = 650 to 685, there is a characteristic blip in the (2,1) magnetic energy, which jumps by 50% , see Fig.6. Ref.22 attaches great

importance to the blip, regarding it as providing an indicator of convergence with N_m. However, the (2,1) energy has already grown by many orders of magnitude since the start of the calculation, and in any case 11 mode computations do eventually exhibit it (see below).

The magnetic energy spectrum is at its flattest around t=700-800 (Fig.5b); thereafter modes furthest from the line of helicity (2,1) in (m,n) space fade, until at time t = 1200 (figure 5c) the spectrum looks as it did at time t = 600. The sequence repeats (but less energetically); the spectrum fills up again by time 1350, and flattens as before. By t = 1590 (the end of the run), it is again fading.

Similar repetitive behaviour is exhibited by the inferred loop voltage, defined by

$$V_I = -\frac{1}{2\pi}\frac{d}{dt}\left(\frac{M}{I}\right) \quad . \tag{18}$$

Note that V_I is defined consistently with (11), i.e. it is 2π smaller than V_I of ref.22. Fig.7a shows the time dependence of V_I for the 57 mode case. The $\dot{M}$ and $\dot{I}$ terms contribute almost equally to the large ($\simeq -32$) swing at $t \simeq 700$. V_I then recovers towards zero around t = 750; although $\dot{M}$ stays negative, I increases by about five per cent, resulting in an overshoot to $V_I = 10$. Note that the second negative spike is greatly reduced, reaching only -6.

It is clear that for lengthy intervals of the computation, the energy spectrum is not fully represented. Indeed, for our choice of physical parameters and numerical scheme this is likely to remain so because of finite computer resources. However, some confidence in the structural stability is given by comparisons with computations differing only in the

number of modes chosen. Using the 117 (m,n) modes listed in Table I, we observed broadening and flattening of the spectrum as in the 57 mode case; there is however, a difference in V_I, which now falls only to -27 (cf.Fig.7a). All other features agree qualitatively with the 57 mode result, thus we argue our 57 mode results are as good as if we had used 117. The 117 mode calculation was not pursued beyond t = 709 because of the prohibitive cost.

More surprising are the results for 11 modes, chosen as in Sec.III. Even with such drastic truncation, the only significant difference is timing. The blip in the (2,1) magnetic energy, for example, starts at t = 700, 50 units later than with 117 modes (Fig.6), and the V_I minimum is correspondingly displaced (Fig.7b). The initial negative voltage is larger (-48) than with more modes, and again there are weaker repetitions (at t = 1700 and t = 2440), qualitatively the same as the first.

In addition to structural stability, the mode interactions remain basically unchanged as S and p_m vary. Figs. 1 and 3 differ only in that there is greater smoothness and slower evolution with larger viscosity. Decreasing S has similar effects. All cases show oscillatory behaviour, with bursts of Alfven waves occurring at island overlap.

B. Initial Conditions.

The first phases of the physical problem discussed in Sec.VIA have been studied previously[22]. Direct comparison with Figs.6-8 of Ref.22 and unpublished results (H.R.Hicks et al, Oak Ridge Report ORNL/TM-9127) suggest that our clock is running differently, so that better agreement is obtained if 25-30 units are subtracted from our timings. There are several factors which can account for this small discrepancy, thus we do

not regard it as significant: Firstly, the time integration schemes are such that RSF underestimates the actual viscosity[15], whereas FORBAK overestimates it[14]. Secondly, uncertainties in initial conditions can lead to timing changes of this magnitude. For instance, in the 11 mode, S = 10^5 case cited in Sec.VIA, changing q_0 from 1.344 to 1.34 and r_0 from 0.560 to 0.567 delayed behaviour by approximately 15 units from time 500 onwards. This change is to be compared, for instance, with a 20 percent change in timing introduced by replacing the quartic form by $\rho(r) = 1$.

A second, more important, way in which initial conditions affect the loop voltage is apparent from the discussions of Sec.VIA, where the second transient is a factor 5 less violent than the first. The spectra in both instances have the same shape, but the absolute amount of energy in a mode is an order of magnitude smaller at the latter time. If the transient interaction of strongly unstable tearing modes is to provide a prognostic for disruptions, then the question as to how the strongly unstable initial conditions are prepared must be clearly resolved.

C. Boundary Conditions.

Constant current boundary conditions are more appropriate to tokamak operation than constant voltage conditions. The 11 and 57 mode runs of Sec.VIA were repeated with fixed current boundary conditions.

The energy spectrum for the 57 mode case develops identically to the constant voltage case until t = 900; thereafter, it shrinks more rapidly and by t = 1255 is totally dominated by modes of (2,1) helicity, with only two other modes (3,2) and (4,3) possessing significant magnetic energy. The 11 mode calculation suggests long time behaviour will exhibit further bursts of Alfvén wave activity. These bursts persist for shorter

time in the constant current case because the driving Poynting flux term is removed as the voltage goes negative.

Figure 8 compares for the same run the inferred and actual voltage for the 57 mode case. As expected, V_I overestimates V, since $\dot{M}$ leads to Lorentz force energy exchange and ohmic dissipation as well as Poynting flux changes. In addition, V lags V_I. If one takes the pessimistic view that computations should terminate when the spectrum becomes full, then results would only be acceptable for times before the arrow at t = 667. One then has to reject the negative voltage spike (V = -8.75 at t = 705). However, our studies of structural stability, although limited, do suggest that gross features are correct.

VII. SUMMARY

We have produced what are demonstrably the best numerical solutions of the reduced MHD equations at high S(= 10^5). Calculations at S = 10^4 and S = 10^6 show the same qualitative behaviour, so it is plausible that our results apply at the higher S = 10^8 relevant to modern tokamaks. There is no unambiguous evidence that the reduced MHD equations are by themselves capable of explaining any of the main features of disruptions.

We have presented results which show that computations supporting the widely accepted view of 'hard' disruptions can be understood in terms of an unphysical alias feedback mechanism. Quantitative predictions of our theory of this mechanism are confirmed by the numerical simulations. We believe that hard disruption calculations which terminate in a spurious singularity at the large S, small p_m values must be interpreted

cautiously. Our theory and computations show how to adjust parameters or to alter the numerical scheme to ensure that solutions remain physically well behaved.

We have undertaken computations of tearing mode interactions when unphysical singularities are absent. We have investigated the effect of varying the timestep Δt, the number of mesh points N_g, number of helical modes N_m, S, p_m, initial conditions and boundary conditions. Results were insensitive to timestep size under conditions of linear stability and to radial mesh spacing if nonlinear stability was maintained. The energy monitor provided a simple diagnostic for convergence with Δt and N_g. There is some dependence on N_m, and on S and p_m, although the same gross behaviour was seen for the wide range of parameters tried: 11- 117 modes, $10^4 \leq S \leq 10^6$ and $0.1 \leq p_m \leq 100$. Varying initial and boundary conditions can produce more marked effects.

What we see in our simulations is the response of a system placed in a very unstable state. The natural result is that the system attempts to dispose of its excess energy to its most unstable modes. If this is an inadequate sink, a wide spectrum of modes is forced to grow, the net effect of which is (via a burst of Alfvén wave transients) to modify the current profile. Subsequent behaviour is less violent, and it appears that there is an approach, via further Alfvénic bursts, to a steady equilibrium. The bursts are of shorter duration and equilibrium is approached more rapidly for constant current boundary conditions, as in that instance more of the excess magnetic energy can be deposited in the external circuit.

It must be made clear that we cannot be precise as to all details, as we do not fully represent the spectrum of Alfvén waves that appear in the transient bursts. Well-resolved MHD calculations in a slightly different context support our overall picture[26]. The major question left unanswered by the lack of resolution concerns the magnitude of the loop voltage swing. We find it reduces as the number of helical modes N_m increases, so will it remain significant as $N_m \to \infty$? This question will be resolved only by employing numerical methods which do not have costs scaling as N^2.

Two features of our calculations may be of importance in understanding disruptions: the Alfvén wave bursts and nonlinear oscillations of low (m,n) (particularly (2,1) and (3,2)) modes. However, the picture is yet far from complete. The assumption that ergodic magnetic fields cause loss of confinement relies on fields remaining ergodic for sufficiently long. We observe transient bursts; brief interludes of broken magnetic surfaces may have little effect on confinement. Moreover, we have shown that small changes in initial conditions (such as produced by the first Alfvén burst) alter quantitative behaviour by an order of magnitude. The results reported herein indicate that two key points require clarifying: the nature of the (1,1) and (2,1) interaction in the preparation of strongly unstable conditions and the interplay between Alfvén wave bursts and transport.

References

1. J.F.Drake and R.G.Kleva, Are major disruptions in tokamaks caused by vacuum bubbles? Phys. Rev. Lett. 53, 1465-1468 (1984).

2. J.P.Dahlbug, D.Montgomery, and W.H.Matthaeus, Turbulent disruptions from the Strauss equations, J.Plasma Phys. 34, 1-46 (1985).

3. M.F.Turner and J.A.Wesson, Transport, instability and disruptions in tokamaks. Nucl.Fus.22, 1069-1078 (1982).

4. J.A.Wesson, A.Sykes, and M.F.Turner, Tokamak disruptions. CLM-R233 (1982).

5. B.V.Waddell, B.A.Carreras, H.R.Hicks, J.A.Holmes, and D.K.Lee, Mechanism for major disruptions in tokamaks. Phys.Rev.Lett.41, 1386-1389 (1978).

   B.V.Waddell, B.Carreras, H.R.Hicks, and J.A.Holmes, Nonlinear interaction of tearing modes in highly resistive tokamaks. Phys. Fluids 22, 896-910 (1979).

6. B.A.Carreras, H.R.Hicks, J.A.Holmes, and B.V.Waddell, Nonlinear coupling of tearing modes with self-consistent resistivity evolution in tokamaks. Phys. Fluids 23, 1811-1825 (1980).

7. H.R.Hicks, J.A.Holmes, B.A.Carreras, D.J.Tetreault, G.Berge, J.P.Friedberg, P.A.Politzer, and P.Sherwell, Resistive MHD calculations of the disruptive instability, Plasma Phys. and Controlled Nuc.Fus. Res., Vol.I, (IAEA, Vienna, 1981), pp 255-268.

8. D.Biskamp, and H.Welter, Studies of MHD turbulence in low-β current-driven plasmas, Plasma Physics and Controlled Nuclear Fusion Research 1982, Vol III, (IAEA, Vienna, 1983), pp 373-381.

9. R.B.White, D.A.Monticello, and M.N.Rosenbluth, Simulation of large magnetic islands: A possible mechanism for a major tokamak disruption, Phys. Rev. Lett. 39, 1618-1621 (1977).

10. J.A.Holmes, B.Carreras, H.R.Hicks, S.J.Lynch, and B.V.Waddell, Stabilization of tearing modes to suppress major disruptions in tokamaks, Nuclear Fus. 19, 1333-1342 (1976).

11. H.R.Strauss, Nonlinear three-dimensional magnetohydrodynamics of noncircular tokamaks, Phys. Fluids 19, 134-140 (1976).

12. H.R.Hicks, B.A.Carreras, J.A.Holmes, D.K.Lee and B.V.Waddell, 3-D nonlinear calculations of resistive tearing modes. J.Comp.Phys.44, 46-69 (1981) (Erratum J.Comp.Phys.53, 205 (1984)).

13. S.I.Braginskii, Transport processes in a plasma, Rev.Plasma Phys 1, 205-311 (1965).

14. J.W.Eastwood, Reduced MHD calculations, Culham Laboratory preprint submitted to Comp.Phys.Reports, (1986).

15. J.W.Eastwood and K.I.Hopcraft, Comments on the stability of the RSF three-dimensional MHD plasma simulation algorithm, J.Comp. Phys. 60, 549-557 (1985).

16. J.W.Eastwood and W.Arter, An interpretation of disruptions in tokamak simulations. Culham Laboratory Preprint CLM-P763, submitted to Phys. Rev. Lett.(1986).

17. W.Arter and J.W.Eastwood, The effect of aliasing errors upon numerical solutions of hydrodynamic and magnetohydrodynamic equations, to appear in Transport Theory and Stat. Phys. (1986).

18. P.H.Rutherford, Nonlinear growth of the tearing mode, Phys. Fluids 16, 1903-1908 (1973).

19. R.B.White, D.A.Monticello, M.N.Rosenbluth, and B.V.Waddell, Saturation of the tearing mode, Phys. Fluids 20, 800-805 (1977).

20. R.G.Kleva, J.F.Drake, and A.Bondesron, Coherent nonlinear destabilisation of tearing modes, Phys. Fluids 27, 769-772 (1984).

21. B.A.Carreras, M.N.Rosenbluth, and H.R.Hicks, Nonlinear destabilisation of tearing modes, Phys. Rev.Lett. 46, 1131-1134 (1981).

22. P.H.Diamond, R.P.Hazeltine, Z.G.An, B.A.Carreras, and H.R.Hicks, Theory of anomalous tearing mode growth and the major tokamak disruption, Phys. Fluids 27, 1449-1462 (1984).

23. N.A.Phillips, An example of nonlinear computational instability, The Atmosphere and the Sea in Motion, ed.B.Bolin, (Rockefeller Institute Press, New York,1959), pp.501-504.

24. R.Bogen et al, MACSYMA Reference Manual, Version 10, (Mathlab Group, M.I.T., 1983).

25. J.W.Eastwood and W.Arter, EPIC - beyond the ultimate difference scheme, to appear in Numerical Methods for Fluid Dynamics, eds.M.Baines and K.W.Morton (O.U.P.,1986).

26. J.P.Dahlburg, D.Montgomery, G.D.Dolen, and W.H.Matthaeus, Large scale disruptions in a current-carrying magnetofluid, to appear in J.Plasma Phys. (1986).

TABLE I. The (m,n) modes chosen for the 57 mode calculations are marked with 'o' and those for the 117 mode calculation marked 'o' or 'x'.

m/n	0	1	2	3	4	5	6	7	8	9	10	11	12	13	14	15
30																x
29																
28															x	
27														x	x	
26														x		
25													x	x		
24												x	x	x		
23												x	x			
22											x	x	x			
21										x	x	x	x			
20										x	o	x	x			
19									x	x	x	x				
18									x	o	x	x				
17								x	o	o	x	x				
16								x	o	o	x					
15							x	o	o	x	x					
14							o	o	o	x	x					
13						x	o	o	o	x						
12					x	o	o	o	x							
11					x	o	o	o	x							
10					o	o	o	o								
9				x	o	o	o	x								
8				x	o	o	o									
7			x	o	o	o	o									
6		x	o	o	o	o										
5		x	o	o	o	x										
4	x	o	o	o	o	x										
3	o	o	o	o	o	x										
2	o	o	o	x												
1	o	o	o	x												
0	o	o	o	x												
-1		x														
-2		x														

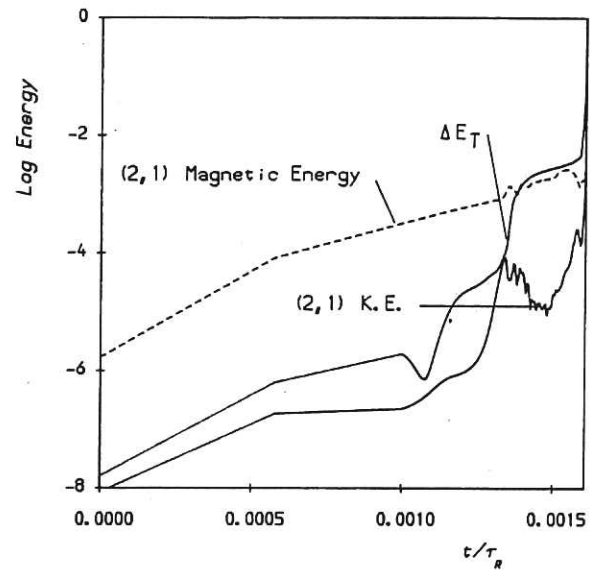

(a)

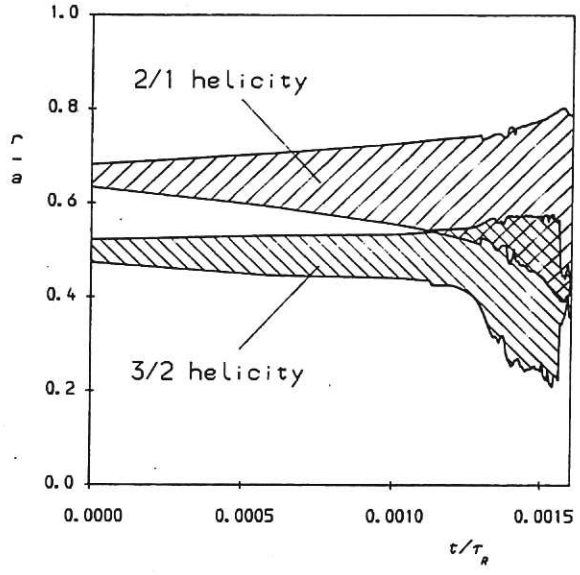

(b)

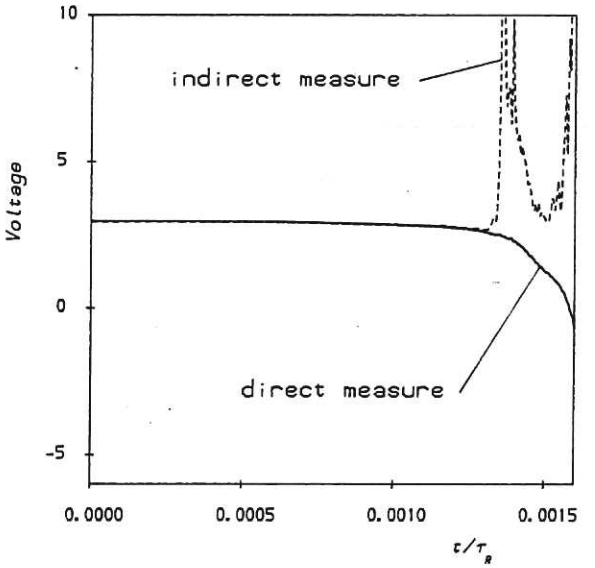

(c)

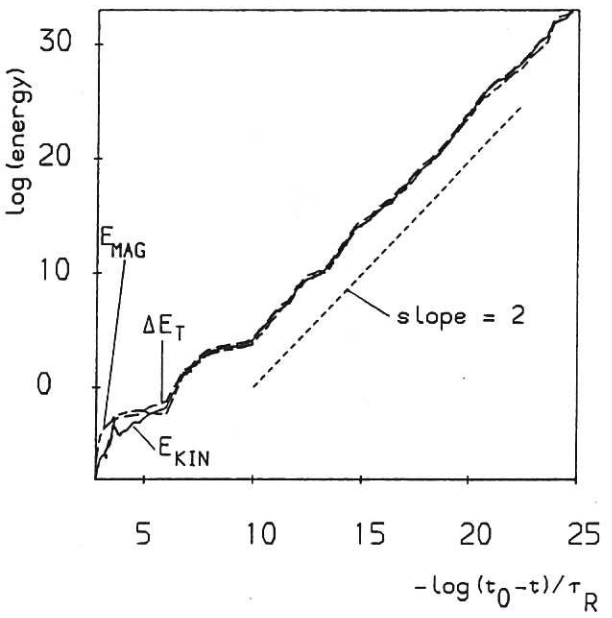

(d)

Fig. 1 S=10^6, p_m=0, ρ=1 and total current held constant, using 11 helical modes and 100 radial mesh-points. Time is measured in units of $\tau_R = a^2/\mu_o$. (a) The deviation from total energy conservation ΔE_T, and the kinetic and magnetic energy of the (2,1) helical mode plotted versus time. Energy conservation becomes poor well before the final blow up. (b) Time-dependence of island widths w. For clarity not all $w \neq 0$ are plotted. (c) Loop voltage as a function of time. The indirect measure assumes energy conservation. (d) Total magnetic energy, E_{MAG}, kinetic energy, E_{KIN} and ΔE_T plotted as functions of time $(t_0\text{-}t)/\tau_R$, demonstrating $\propto (t_o\text{-}t)^{-2}$ behaviour. t_o is the time at which the stability criterion, Eq.(7) forces Δt to zero.

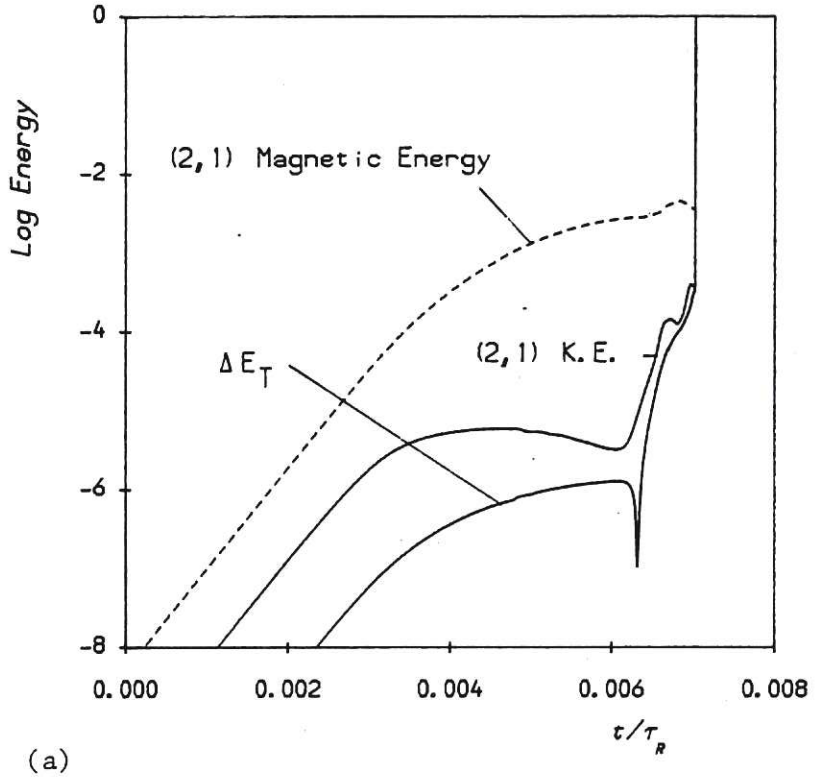

(a)

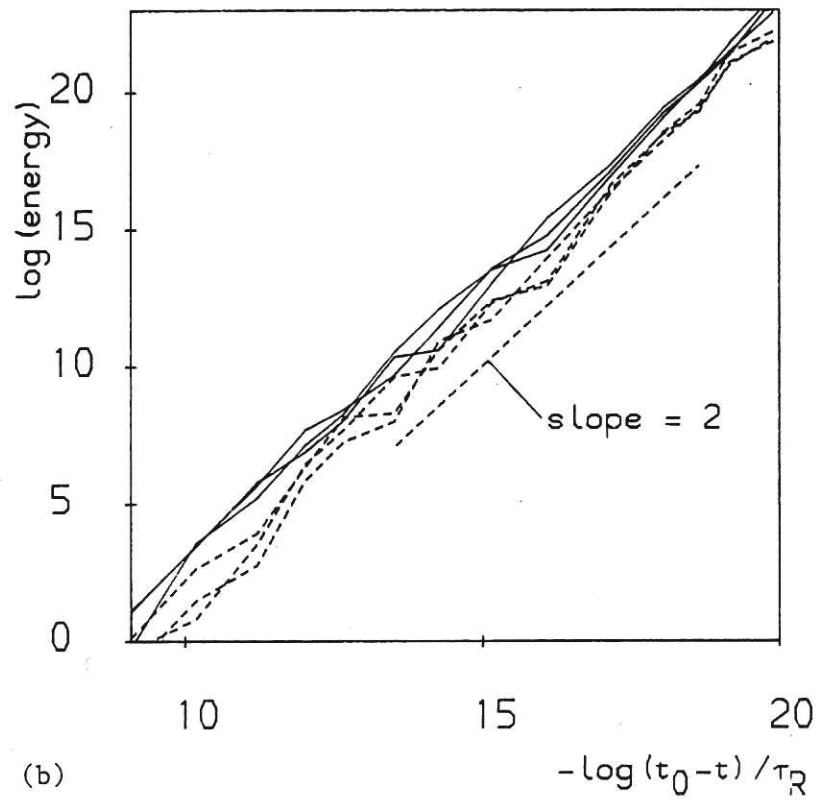

(b)

Fig. 2 $S=10^5$, $p_m=1$, $\rho(r)$ and constant voltage boundary conditions, using 57 helical modes and 200 radial mesh-points. (a) ΔE_T, and the kinetic and magnetic energy of the (2,1) mode plotted against time. (b) Magnetic energies, drawn dashed, and kinetic energies, drawn full, for the (2,1), (3,2) and (5,3) helical modes, demonstrating $\propto(t_o\text{-}t)^{-2}$ behaviour.

CIM-P779

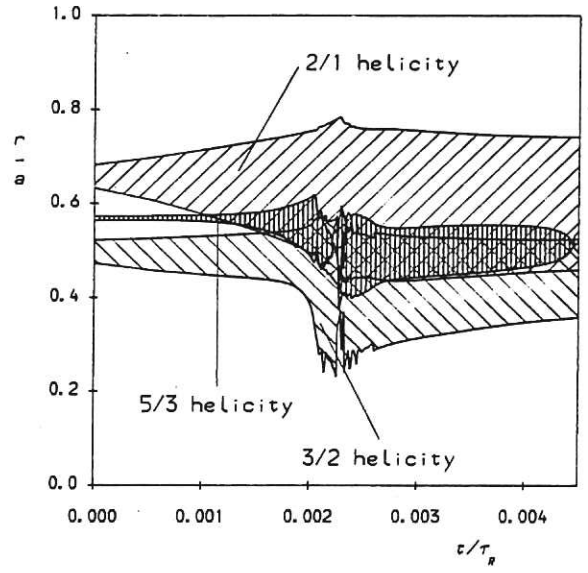

(a)

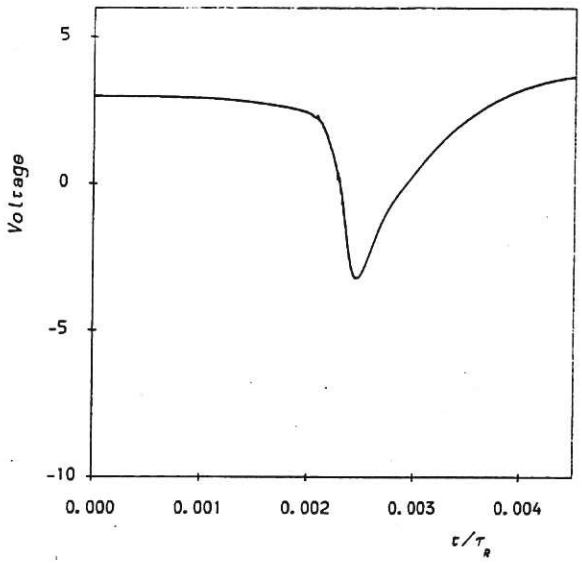

(b)

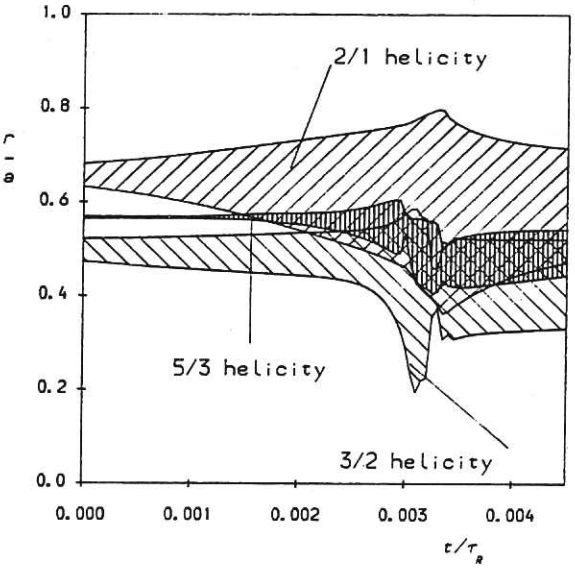

(c)

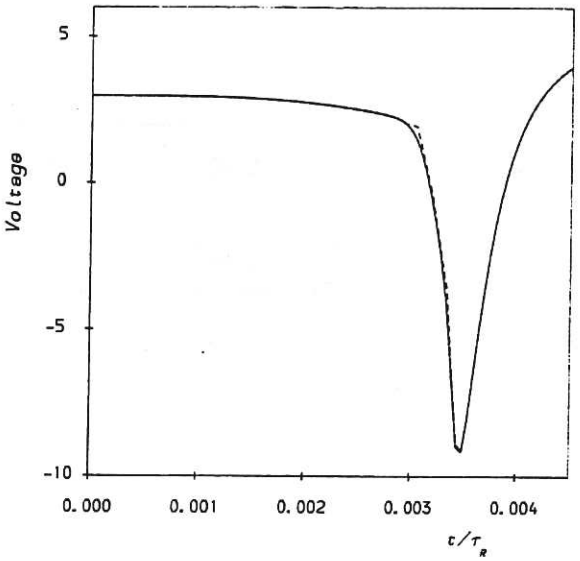

(d)

Fig. 3 $S=10^6$, $p_m=10$ (a and b) or $p_m=100$ (c and d), $\rho=1$ and total current held constant, using 11 helical modes and 100 radial mesh-points. (a) and (c) Time-dependence of island widths w of the three principal islands. (b) and (d) Loop voltage as a function of time. The indirect measure (drawn dashed) is virtually indistinguishable from the direct measure.

CLM-P779

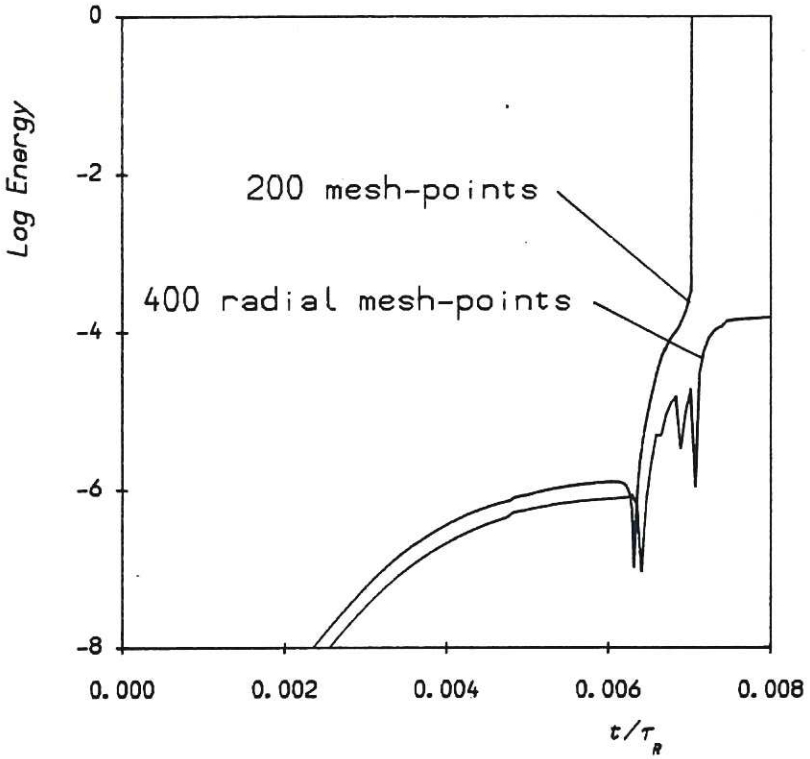

Fig. 4 As in Fig. 2, $S=10^5$, $p_m=1$, $\rho(r)$ and constant voltage boundary conditions, using 57 helical modes. The deviation from total energy conservation, ΔE_T, is plotted for runs with 200 and 400 radial mesh-points.

CLM-P779

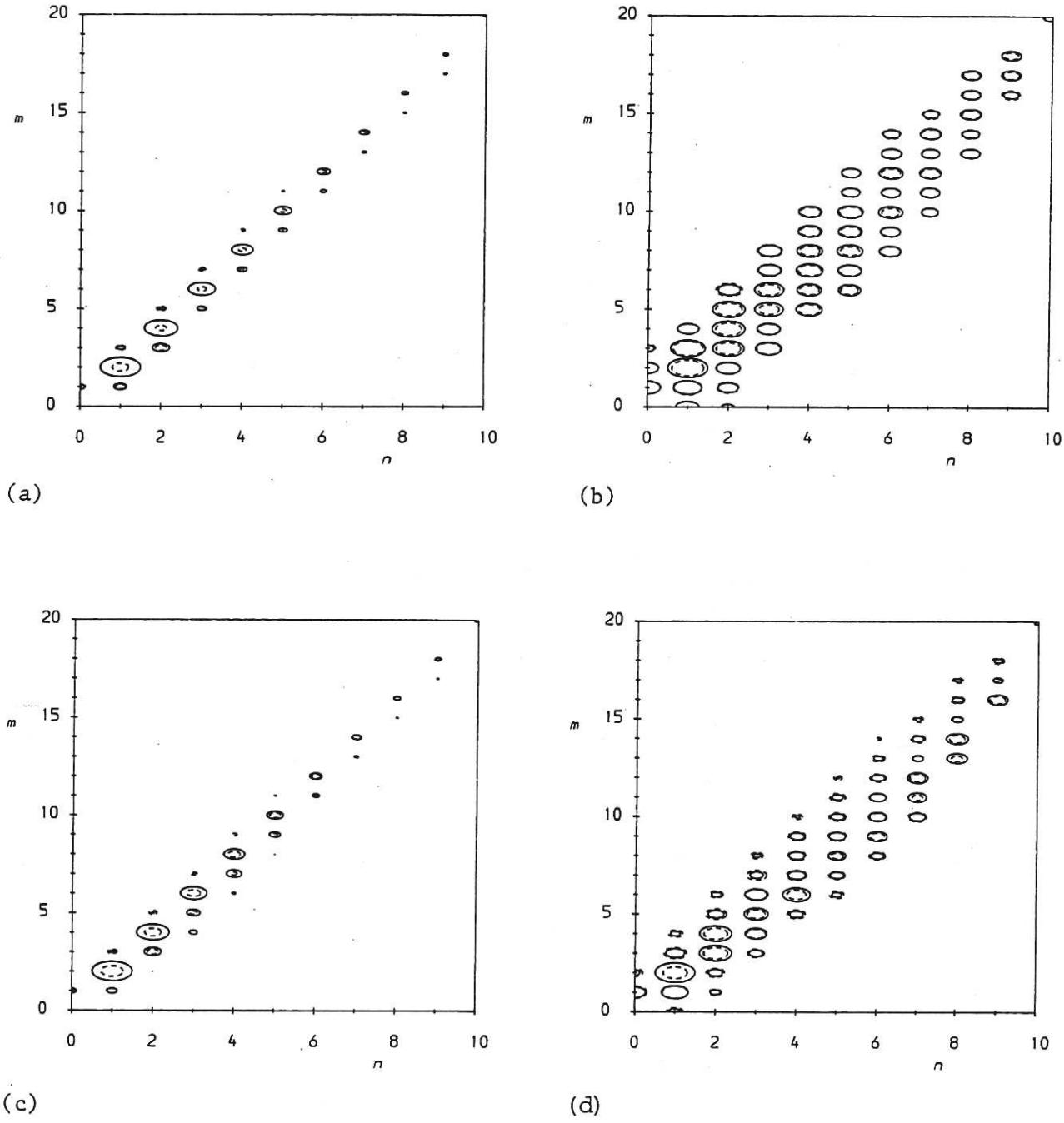

Fig. 5 Same case as Fig. 2, but using 400 radial mesh-points. The magnetic (full line) and kinetic (dashed line) energy spectrum drawn at a sequence of times (a) 601, (b) 730, (c)1202 and (d) 1362.5, in Alfvén units. Following ref. 22, the linear dimensions of each ellipse are proportional to $\log_{10}(E_M \times 10^5 / \max(E_M))$ and the (0,0) and very weak modes are omitted.

CLM-P779

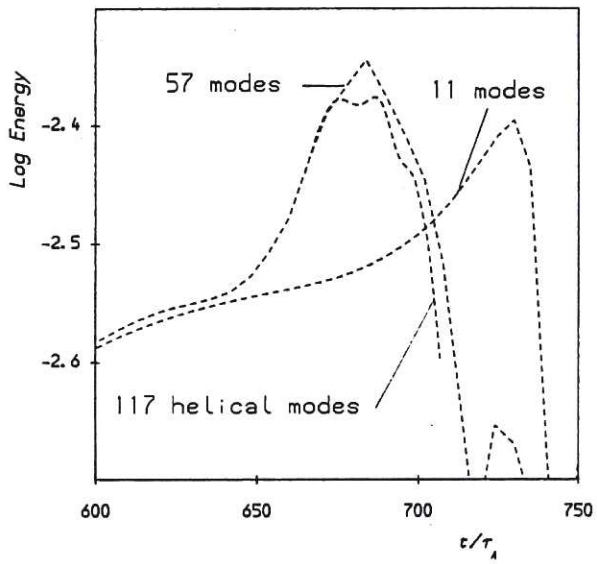

Fig. 6 Same case as Fig. 4: the magnetic energy in the (2,1) mode plotted versus time in Alfvén units for calculations with (number of helical modes, number of radial mesh-points) = (11,200), (57,400), (117,400).

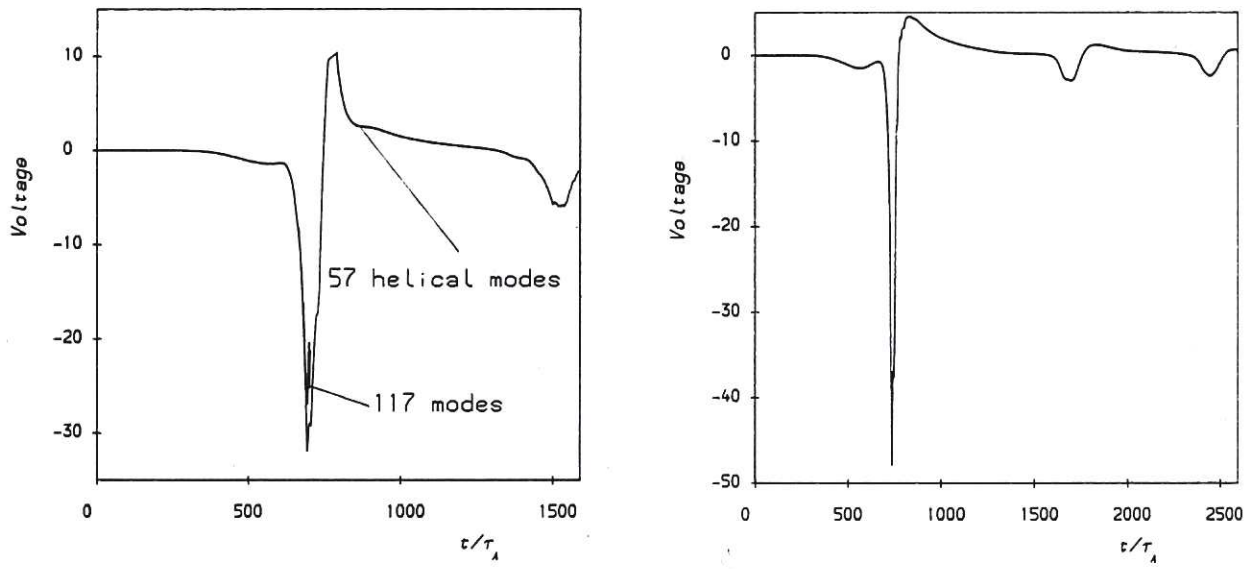

Fig. 7 Loop voltage plotted versus time in Alfvén units for the computations of Fig. 6. (a) 57 and 117-mode runs superimposed, (b) 11-mode run.

CLM-P779

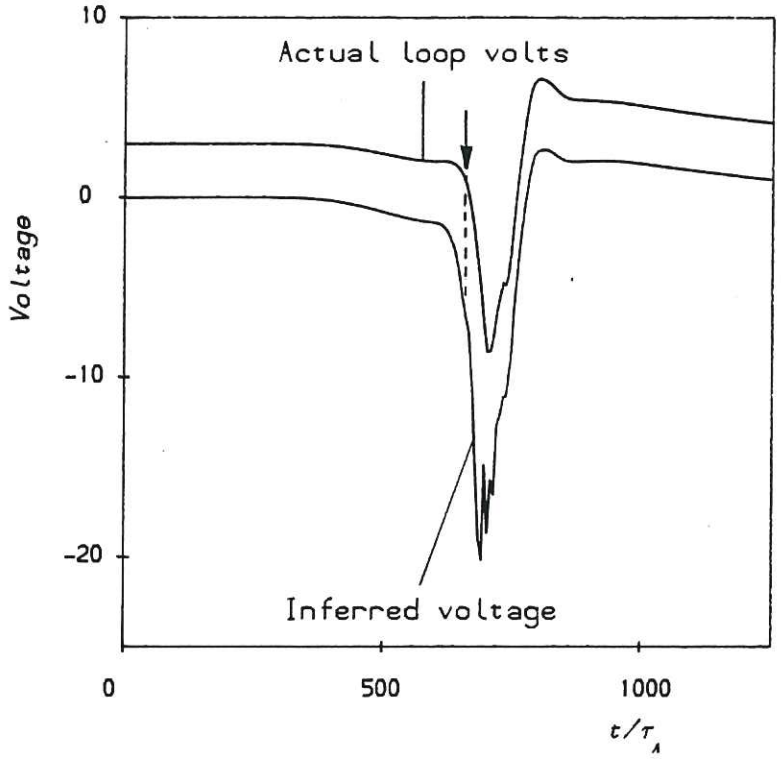

Fig. 8 $S=10^5$, $p_m=1$, $\rho(r)$ case, but with constant current boundary conditions. Ng=400 and 57 helical modes were employed. The inferred (Eq. 18) and actual loop voltages plotted on the same scale. The arrow at $t=667$ indicates the point at which the spectrum becomes full.

CLM-P779